Polish Journal of Medical Physics and Engineering
The Journal of Polish Society of Medical Physics
ISSN 1898-0309, doi: 10.2478/pjmpe-2024-0016

September 2024
Vol 30, Issue 3

Scientific Paper

An Optimal Framework for the Effective Delivery of the Radiation to the target by Considering the Case of Head and Neck Cancer

Pushpendra SINGH [1,ABCDEF,*], Naveen Kumar DEWANGAN [1,B], Ravindra Manohar POTDAR [1,E], Seema SINGH [2,AC], Alka MISHRA [3,BD], Santosh Kumar MISHRA [4,EF]

[1]*Department of Electronics & Telecommunication Engineering, Bhilai Institute of Technology, Durg, India*
[2]*Department of Electronics & Telecommunication Engineering, Shri Shankaracharya Technical Campus, Bhilai, Chhattisgarh, India*
[3]*Department of Electrical & Electronics Engineering, Bhilai Institute of Technology, Durg, India*
[4]*Department of Mechanical Engineering, Bhilai Institute of Technology, Durg, India*
[*]*Corresponding author: Prof. Pushpendra Singh: pushpendra.singh@bitdurg.ac.in*

(received 11 August 2023; accepted 27 June 2024)

Abstract

Introduction: Delivering the required dose to the intended target while limiting the radiation's impact on adjacent normal tissue is the principal goal of radiotherapy. One effective method for doing this is intensity-modulated radiotherapy, which operates on the idea of inverse planning. In order to transmit the fluence to the target efficiently while sparing the healthy cells, the objective of the research is to generate the ideal radiation dosage by first optimizing the fluence and then adjusting the trajectory of the leaf.

Materials and Methods: Fluence mapping is utilized in inverse planning to calculate each beam's intensity level. Considering dose-volume limitations on the OARs, five evenly spaced beams expose the intended target for examination. The efficacy of the therapy regimens was measured using cumulative DVH. We have taken into account a number of PTVs and OARs acquired from the CORT dataset, which is accessible publicly for the benefit of researchers, to validate our approach.

Results: For the various target area and critical organs, we fixed the radiation levels at 82 Gy and 61 Gy across the PTV-70 and PTV-56, and similarly, the dose volumes of 52 Gy, 40 Gy, and 32 Gy across the Spinal Cord, Spinal Cord PRV, and Left and Right Parotid. Analysis of the data indicates that our approach generates the highest D95 dosage level possible across the target area for each PTV. Additionally, relative to other approaches employed in the literature, our approach's duration for analysis (254.28 Seconds) is extremely low.

Conclusion: The suggested approach can produce global minima for IMRT planning with consistent quality across a range of treatment plans and effectively improve safety for substantial dual OARs.

Keywords: fluence map optimization; planned target volume; radiotherapy; leaf trajectory optimization.

Introduction

Around 650-700 thousands of fresh cases of head and neck cancer (HNC) are identified each year, accounting for 5-6% of the total number of cancer diagnoses globally.[1] The most typical kind of HNC, with a global frequency of 300 occurrences per 1,000 individuals[2], has originated in the pulp chamber.[3] An oncologic priority is figuring out how to provide care and cure cancer patients as effectively as possible. Radiotherapy (RT) is one of the major forms of therapy to treat HNC, along with chemotherapy and surgery.[4]

The main goal of radiotherapy is to deliver the necessary dosage to the intended area while minimizing radiation's impact on nearby normal cells.[5] Various types of radiation therapies have discussed by the authors in the literature for planning and proficiently delivering extremely conformal dosage to the target while concurrently sparing the adjacent OARs to a larger amount. Intensity-modulated radiotherapy is one of the powerful tool to do so. IMRT has the capability to deliver the variable amount of radiation dosage to the planned targets by using the property of intensity modulation. IMRT works on the principle of inverse planning in which at first outlined the structural allocation, upper and lower dose bounds to each of the allocated portion and beam positions.[6] Then using iterative calculations will compute the beamlet strengths and at last apply multiple optimization techniques that can distribute the preferred dose response.

Authors' contribution: A – Research concept and design, B – Collection and/or assembly of data, C – Data analysis and interpretation, D – Writing the article, E – Critical revision of the article, F – Final approval of the article.

Fluence mapping is a significant process for inverse planning.[7-10] An effective fluence map optimization has two essential characteristics. First, the dosage suggested should be administered in its entirety and dispersed evenly among the intended target areas. Second, the amount of radiation given should have little to no impact on normal cells nearby the intended location. In particular, the spreading of doses across OARs ought to stay below the maximum permissible dose limit advised by an oncologist.[11] Numerous studies have been published in the literature that take these restrictions into account, with the majority of them focusing on the building of models employing dose-volume limitations[12] and related methods for the computation of results. The majority of the mathematical frameworks developed by the researchers comprise either regular or nonlinear computational models, keeping in mind the difficulty of the procedure and the size of the problem.[13] In these frameworks, two terms—sum of relative dose rate and the sum of square dose value—have been utilized most frequently throughout the study to define the intended area. Dose-volume restrictions have been widely employed for OARs.

Numerous methods are available in literature for modeling of FMO including linear[14-15], non-linear[16] and quadratic programming[17]. Out of these methods, linear methods are dominant one but it requires the initialization of integer variables. The immediate incorporation of DVCs into the FMO framework is not possible without initializing integer values. Since only a DVC determines the quantity of medication to be given to a particular quantity of voxels within the framework, precise estimation of the total number of voxels meeting the DVC's requirements is, in fact, a non-convex combinatorial issue that produces numerous local minimums, making it difficult to determine the global minimum.[18]

Once DVCs have been applied to the model, non-linear approaches can be used to provide the local optimum or suboptimum results.[19] However, to distinguish between these local and global optima, there isn't enough data on the research gap. For the purpose of addressing the aforementioned issue, the author of reference[20] employs an approximation and a convex objective function. The global minima are then simply created. On the differential DVH for approximating DVCs, they integrated the limitations on conditional value at risk. The author of reference[21] uses linear methods to incorporate dose-volume bounds and optimize the beam weights.

Modelling with dose-volume constraints are non-convex optimization issues[22-23], therefore, the analysis of these models is difficult in nature. The authors have offered numerous patterns and methods in the literature to formulate this issue. By utilizing the cVar notion, the author of reference[24] created a non-convex framework from a model that is linear. The authors of reference[25] employed an optimization model with multiple dose-volume constraints, while in publication[26] developed a least-squares framework that utilized a discrete objective function. Researchers have proposed a variety of mathematical model-centered computational methods for resolving problems, including gradient algorithms[27] and analytical algorithms like simulated annealing and genetic algorithms[28]. Additionally, in order to achieve the necessary dose-volume arc, authors of [29] and [30] applied an optimization technique based on voxel-dependency. Additionally, authors of [31] projected a concept of dosimetric capacity, which was integrated into the IMRT procedure.

The subsequent sections comprise the remaining portions of the article. In Section 2: Materials and Methods, we developed the Fluence map optimization model for radiotherapy treatment scheduling around various dose-volume limitations. Besides the basic radiation therapy illustration, we have also developed an optimization method. In Section 3: Results, there is a description of the dataset utilized for the problem analysis, followed by a presentation of the simulation-based analysis of the problem. Lastly, in Section 4, Conclusion, we summarize the findings and go through potential next research avenues.

Materials and Methods

Notation and Preliminaries

Euclidean Space: We analyse the induced norm $\|\cdot\|$ and a Euclidean space defined by $\mathbb{R}^n$ with an internal product $\langle\cdot,\cdot\rangle$. The adjoint $D^T: \mathbb{R}^n \to \mathbb{R}^m$ is the unique linear map satisfying a linear map $D: \mathbb{R}^n \to \mathbb{R}^m$.[32]

$$\langle Dq,\ p\rangle = \langle p,\ D^T q\rangle \text{ for all } p \in R^n,\ q \in R^m \quad \text{Eq. 1}$$

Where the norm of D is stated as $\|D\| = \max_x \|Dx\|$, which matches with D's maximum singular value and fulfills $\|D\| = \|D^T\|$.

Functions and Geometry: minimizing a bounded function over a subgroup of $\mathbb{R}^n$ resemble one-to-one with a challenge of minimizing over all of $\mathbb{R}^n$ a function $f: \mathbb{R}^n \to \overline{\mathbb{R}}$, under the identifications:

dom f	=	A group of viable solutions
argmin f	=	A group of optimal solutions
inf f	=	The best possible result.

Thus, under such scenario

$$dom\ f = \{p \in R^d : f(p) < \infty\} \quad \text{Eq. 2}$$

And,

$$epi\ f = \{(p,\mu) \in R^d \times R : \mu \geq f(p)\} \quad \text{Eq. 3}$$

The epigraph therefore comprises of all the points of $\mathbb{R}^{d+1}$ situated on or beyond the curve of f. (It's worth noting that $epi\ f$ is actually a subgroup of $\mathbb{R}^{d+1}$, not just of $\mathbb{R}^d \times \overline{\mathbb{R}}$).[33] The appearance of $epi\ f$ under the projection $((p,\mu) \to p$ is $dom\ f$. Here if $f(p) = \infty$ means line missing $epi\ f$ and if $f(p) = -\infty$ means line is entirely included in $epi\ f$.

Lipschitz Continuity: For any map $F: \mathbb{R}^n \to \mathbb{R}^m$, we have

$$lip(F) = \sup_{p \neq q} \frac{\|F(p)-F(q)\|}{\|q-p\|} \quad \text{Eq. 4}$$

Here if the inequality $lip(F) \leq M$ exists, F is Lipschitz Continuous for $M \geq 0$.[34]

Proximal Mapping: For any real value function f, the proximal mapping defined by,[35]

$$prox_{\psi f}(p) = \underset{z}{\operatorname{argmin}} \left\{ f(z) + \frac{1}{2\psi} \|z-p\|^2 \right\} \quad \text{Eq. 5}$$

Problem Formulation

Now as we now due to the inverse nature of the fluence mapping problem, we must ascertain the ideal beamlet intensities for a given dosage over the target malignant volume and healthy cells. The nomenclature of various parameters of the mathematical framework is as follows:

We divided complete voxels under two types of areas: A group of target areas $T_i = \{T_1, T_2, T_3, \ldots . T_u\}$ where T_i specifies the i-th target area, u specifies the quantity of target states and the corresponding voxel sizes are $S_{T_i} = \{S_{T_1}, S_{T_2}, S_{T_3}, \ldots . S_{T_u}\}$. A collection of non-intended voxels $N_j = \{N_1, N_2, N_3, \ldots . N_v\}$, where N_j represents the jth non-intended voxels, v indicates the sum of non-intended voxels (including strong tissues and acute structures), the equivalent voxel size are $S_{N_j} = \{S_{N_1}, S_{N_2}, S_{N_3}, \ldots . S_{N_v}\}$. Likewise, pixels are used to segment the radiation level profiles of the corresponding beams. With the help of the collimator, we can calculate pixel size. All of the pixel data are thought to be contained in column vector H. We establish a correlation between each voxel's volume and its corresponding pixel's intensity in the vector of column L with the aid of a precise matrix. Consider that the intended voxels are represented by the matrix $F_T = \{F_{T_1}, F_{T_2}, F_{T_3}, \ldots . F_{T_u}\}$, and the non-target voxels are represented by the matrix $F_N = \{F_{N_1}, F_{N_2}, F_{N_3}, \ldots . F_{N_u}\}$. As a result, the dose absorbed by the intended voxels is represented by the expression $D_T = F_T . H$ and the dose absorbed by the non-target voxels by the expression $D_N = F_N . H$, where a vector of intensity is denoted by H. The suggested dosage amount for intended volume T are $D_{TP_i} = \{D_{TP_1}, D_{TP_2}, D_{TP_3}, \ldots . D_{TP_u}\}$ and the higher dosage limitations for non-intended volume N are $D_{NU_j} = \{D_{NU_1}, D_{NU_2}, D_{NU_3}, \ldots . D_{NU_u}\}$.

By taking into account the maximum dose limitations on the PTV, the ideal problem of fluence map optimization considering the limitations on OAR and PTV can now be further articulated as,

$$\begin{aligned} &\text{minimize} && \sum_{i=1}^{u} \frac{p_i}{S_{T_i}} \left(D_{T_i} - D_{TP_i}\right)^2 \\ &\text{Subjected to} && D_{N_j} \leq D_{NU_j} \\ & && H \geq 0 \end{aligned} \quad ; \text{for } j = 1,2, \ldots, v \quad \text{Eq. 6}$$

In the proposed plan, the supplementary parameter y_N are used to fulfil the dose-volume requirements, whereas the residuals $D_{N_j} - D_{NP_j}^{tol}$ tol may or may not. In an epigraphical sense, the weights p_j regulate how closely y_N must approximate $D_{N_j} - D_{NP_j}^{tol}$, and as $p_j \to \infty$, the problem converges to the idealized form.

Lemma 1: For any y', y from $\mathbb{R}^n$ we have,

$$f(y) - f(y') - [f'(y'), (y-y')] \leq \frac{p_j}{2S_{N_j}} \|y - y'\|_2^2 \quad \text{Eq. 8}$$

Proof:

For all $y', y \in \mathbb{R}^n$ we have,

$$f(y) = f(y') + \int_0^1 \left[f'\left(y' + \varphi(y-y')\right), y-y'\right] d\varphi \quad \text{Eq. 9}$$

$$= f(y') + [f'(y'), y-y'] + \int_0^1 \left[f'\left(y' + \varphi(y-y')\right) - f'(y'), y-y'\right] d\varphi \quad \text{Eq. 10}$$

Therefore,

$$|f(y) - f(y') - [f'(y'), y-y']| = \left| \int_0^1 \left[f'\left(y' + \varphi(y-y')\right) - f'(y'), y-y'\right] d\varphi \right| \quad \text{Eq. 11}$$

$$\leq \int_0^1 \left| \left[f'\left(y' + \varphi(y-y')\right) - f'(y'), y-y'\right] \right| d\varphi \quad \text{Eq. 12}$$

$$\leq \int_0^1 \left\| f'\left(y' + \varphi(y-y')\right) - f'(y') \right\| * \|y-y'\| \, d\varphi \quad \text{Eq. 13}$$

$$\leq \int_0^1 \left\| f'\left(y' + \varphi(y-y')\right) - f'(y') \right\|_2 * \|y-y'\|_2 \, d\varphi \quad \text{Eq. 14}$$

$$\leq \frac{p_j}{2S_{N_j}} \|y - y'\|_2^2 \quad \text{Eq. 15}$$

Convergence Analysis:

Let's consider that $f: \mathbb{R}^n \to \mathbb{R}$ is both convex and differentiable and furthermore,

$$\|f'(h) - f'(y)\| \leq \frac{S_{Nj}}{p_j} \|h - y\| \quad \text{Eq. 16}$$

For any h, y i.e., f' is Lipschitz continuous with $\frac{S_{Nj}}{p_j} > 0$.

Theorem 1: Gradient descent by considering a predermined step size $d_j \leq \frac{S_{Nj}}{P_j}$ fulfils,

$$[f(h^k) - f(h^*)] \leq \frac{\|h^0 - h^*\|^2}{2kd_j} \quad \text{Eq. 17}$$

i.e., we reach an ε accurate solution in $O(1/\varepsilon)$ relations.

Proof:

Since f′ Lipschitz with constant $\frac{S_{Nj}}{p_j}$, which means $\frac{S_{Nj}}{p_j} I \geq f''$, we have $\forall h, y, z$.

$$(h-y)^T * \left(f'' - \frac{S_{Nj}}{p_j} I\right) * (h-y) \leq 0 \quad \text{Eq. 18}$$

Which means,

$$\frac{S_{Nj}}{p_j} \|h-y\|^2 \geq (h-y)^T * f''(z) * (h-y) \quad \text{Eq. 19}$$

Based on Taylor's remainder theorem, we have $\forall h, y, \exists z \in [h, y]$

$$\therefore f(y) = f(h) + f'(h)^T(y-h) + \frac{1}{2}(h-y)^T f''(z) * (h-y) \quad \text{Eq. 20}$$

$$\leq f(h) + f''(h)^T(y-h) + \frac{S_{nj}}{2p_j}(h-y)^T\|y-h\|^2 \quad \text{Eq. 21}$$

Plugging in $h^+ = h - t * f'(h)$,

$$f(h^+) \leq f(h) + f'(h)^T\left(h - d_j h' - h\right) + \frac{S_{nj}}{2p_j}\left\|h - d_j h' - h\right\|^2 \quad \text{Eq. 22}$$

$$= f(h) - \left(1 - \frac{S_{nj}}{2p_j} d_j\right) - d_j\|f'(h)\|^2 \quad \text{Eq. 23}$$

Taking $0 < d_j \leq \frac{p_j}{S_{nj}}$, $1 - \frac{S_{nj}}{2p_j} d_j \geq \frac{1}{2}$, we have

$$f(h^+) \leq f(h) - \frac{t}{2}\|f'(h)\|^2 \quad \text{Eq. 24}$$

Since f is convex,

$$f(h) \leq f(h^*) + f'(h)^T(h - h') \quad \text{Eq. 25}$$

We have

$$f(h^+) \leq f(h) - \frac{d_j}{2}\|f'(h)\|^2 \quad \text{Eq. 26}$$

$$f(h^+) \leq f(h^*) + f'(h)^T(h-h') - \frac{d_j}{2}\|f'(h)\|^2 \quad \text{Eq. 27}$$

$$= f(h^*) + \frac{1}{2d_j}(\|h-h^*\|^2 - \|h - h^* - tf'(h)\|^2 \quad \text{Eq. 28}$$

$$= f(h^*) + \frac{1}{2d_j}(\|h-h^*\|^2 - \|h^+ - h^*\|^2 \quad \text{Eq. 29}$$

Summing over iterations, we have

$$\sum_{i=1}^{k}(f(h^i) - f(h^*)) \leq \frac{1}{2d_j}(\|h^0 - h^*\|^2 - \|h^k - h^*\|^2 \quad \text{Eq. 30}$$

$$\leq \frac{1}{2d_j}\|h^0 - h^*\|^2 \quad \text{Eq. 31}$$

From **Equation 30** we can see that $f(h^k)$ is non-increasing, then

$$f(h^k) - f(h^*) \leq \frac{1}{k}\sum_{i=1}^{k}(f(h^i) - f(h^*)) \leq \frac{\|h^0 - h^*\|^2}{2kd_j} \quad \text{Eq. 32}$$

The optimization algorithm

In the function used for re-weighting the final outcome, the algorithm applied the concept of block coordinate descent. Implemented the fundamental of variation in penalty decomposition for the convex-cordiality problem. The algorithm can be described as follows:

1. Initialize the value of iteration m , weight factor α and internal stopping tolerance ε, for the organ at risk.
2. Solve the FMO model.
3. If error generated is greater than stopping tolerance criteria, calculate $(m+1)^{th}$ value of h and y by using block coordinate descent approach for the m^{th} value of h and y.
4. Re-calculate the value of error function by using the $(m+1)^{th}$ value of h and y generated in step-3.
5. For entire values of dose-volume bound, calculate the $(m+1)^{th}$ value of α by multiplying it by weight update parameter.
6. Calculate the $(m+1)^{th}$ value of ε by multiplying it by stopping tolerance update parameter.
7. Determine the final value of h.
8. If all constraints are satisfied and result is acceptable, stop; otherwise go to step 3.

Leaf Trajectory Optimization

The entire leaf trajectory optimization method is broken down into several parts. The root process of the work done in this module is depicted in **Figure 1.**

In order to create an optimal dosage pattern for the patient's geometry (the location of the tumor and all surrounding organs), we must first set up an optimized fluence map (m) and an additional fluence map placed at predetermined angles around the patient. The procedures described in this section show how to move the MLC's leaves around the field to build an identical fluence map for a specific dose rate sequence.

Our optimization allows the leaves to move back and forth, which is necessary for attaining optimal motions in the context of a general (non-constant) dose rate. Additionally, since these restrictions may not be the best, we let each pair's leaves to start and end at any viable location throughout the field rather than simply at the edges of the treatment area. As a result, the treatment plan we develop here pertains to the constantly changing IMRT field allocation issue, which involves a part of the complete variable VMAT problem.

By fixing the issues with it, we consider a standard two-step process for the best delivery of fluence maps. The fluence maps are optimized initially as part of the optimization issue solution strategy, and then they are delivered via a leaf sequencing

method. In this study, we ignore the preliminary optimization and simply consider that an IMRT optimization produced the fluence maps.

The subsequent features of the therapeutic delivery equipment, a linear accelerator (linac) with an MLC, are also presumptive:

- A constantly changing dose rate that is capped at a given amount.
- MLC leaf velocities vary constantly all the way to their peak value.

In addition to ignoring leaf movement, the linac's teeth are not simulated. Furthermore, we presumptively assume that in this stage, leaves will completely have closed and rotate.

Formation of Various Movement Locations

We apply randomization to the various trajectory classes to produce a variety of plausible initial responses, as shown in **Figure 2**.

Each of the trajectories shown above was produced for different timing cycle by varying the position of the leaf. To produce a random practical right to left trajectory, for instance, we rotate the wheel at each subsequent step to determine whether a leaf would move at the fastest rate towards the left or stay still. Leaf movements could alternatively be generated randomly using numerous patterns. We check the feasibility of the leaves by checking that they do not collide or extend outside their boundaries. The radiation levels are chosen at D_{max}.

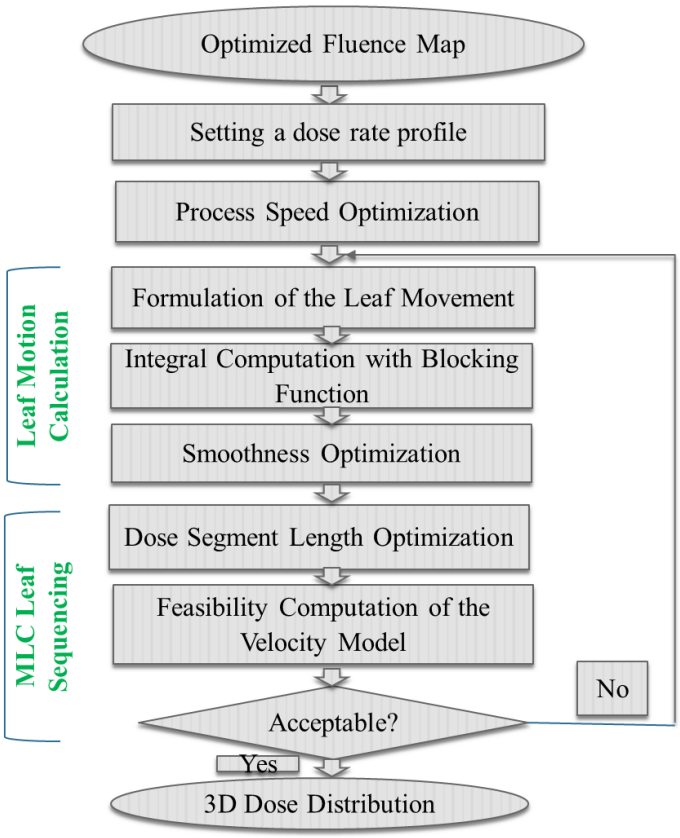

Figure 1. Root process of the leaf trajectory optimization

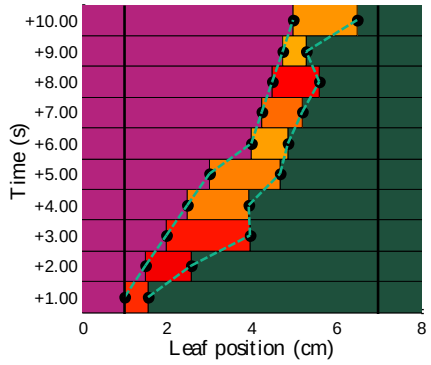

(a) Leaf Movement for T = 3.5 Sec

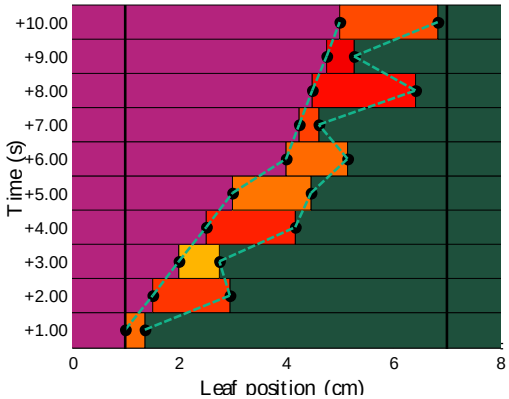

(b) Leaf Movement for T = 4 Sec

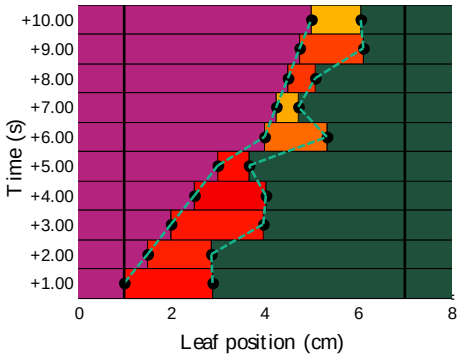

(c) Leaf Movement for T = 4.5 Sec

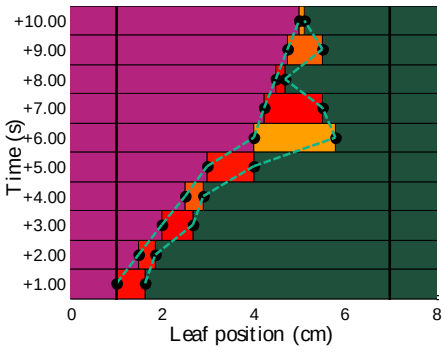

(d) Leaf Movement for T = 5 Sec

Figure 2. Left and Right leaf trajectories under different time

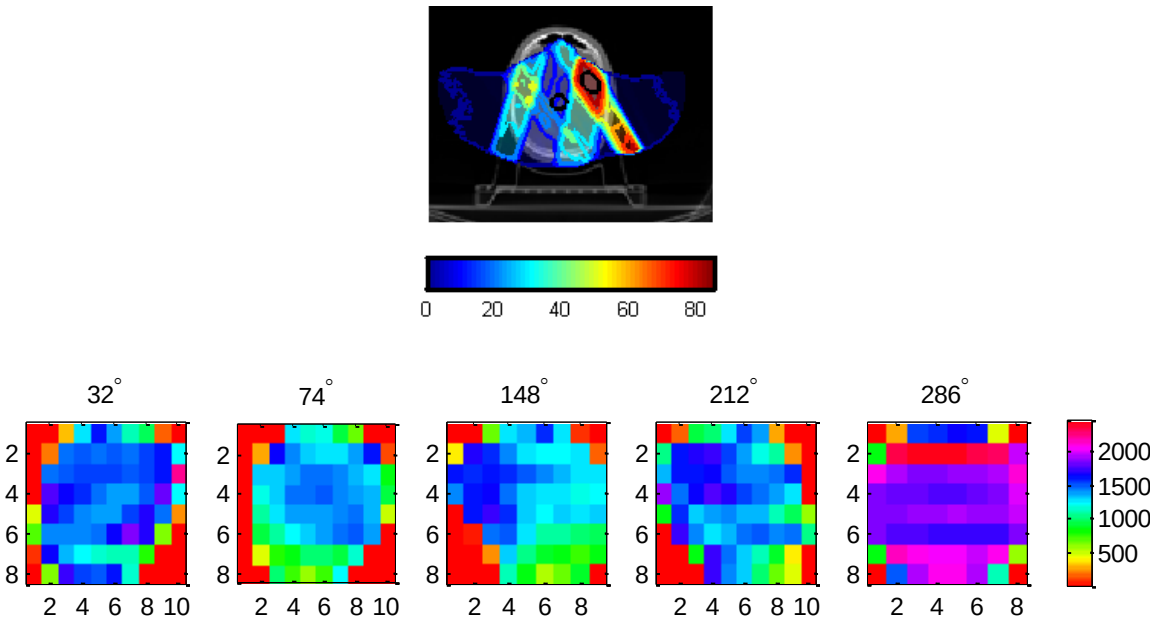

Figure 3. By ensuring that the PTVs receive almost uniform radiation of 60 Gy and that the OARs receive approximately the specified dose, the best treatment strategy was achieved for the beamlet intensity (MU) of five beams: (a) Five beams that have dose-volume limits on the OARs reveal tumors. (b) Beamlet intensity of five beams

Results

Dataset

Clinical trial data is frequently insufficient or erroneous, resulting in exaggerated healthcare intervention effects. Scientists and editors created the CONSORT statement, a 22-item checklist for writers, editors, reviewers, and readers, to improve quality. It was adopted by a number of publications and editorial boards.[36] Here the CORT dataset was used for the simulation of the formulated problem.[37] The suggested issue was simulated using the head-and-neck scenario. The head-and-neck data comprises 1983 beam angles. By a 0.5 cm × 0.5 cm of beamlet resolution, the total beamlet is 2,257,507. For left-right, anterior-posterior, and superior-inferior, the voxel density and grid dimensions are $(3.0, 3.0, 5)$ mm and $(160, 160, 67)$, respectively. 25,388 and 251,893 are the sum of voxels in the desired location and the body. PTV-56, PTV-63, and PTV-70 are the three primary higher and lower dosage locations, whereas larynx, lips, Liver, Spinal Cord, left and right parotid, left and right optic nerve, and left and right lens are the OARs (see **Figure 3**). For beam angles ranging from 0° to 358°, in intervals of 2°, the collection of data includes a beamlet-to-voxel mapping. The term used for representing beamlet levels in the CORT datasets is monitor units, where for a 10 cm penetration in water at the midpoint of a 10 cm × 10 cm radiation field, 100 MU delivers a dose of 1 Gy.[38] We utilised the function titled minConf_TMP within the minConf library to solve the positive least-squares issues[39] and convex programmes were solved with the CVX package.[40]

The analysis is performed in different steps. First, we start analyzing the results by their minimum complexity and further increase the complexity to its maximum value.

Single Target and Critical Structure with Single Dose-Volume Constraint

We look at the problem of targeting a PTV-56 tumor with a consistent dosage of 75 Gy while adhering to the dose-volume restriction that not exceeding 30 percent of the spinal cord area absorbs in excess of 40 Gy. In this scenario, we use starting spinal cord weight $p_2^{(0)} = 1$, internal ending deviation $\varepsilon^0 = 0.1$, weight adjustment factor $\tau = 2$, concluding deviation adjusting factor $\sigma = 0.95$, and external final deviation $\emptyset = 0.01$. The interior portion of the rectangular section in **Figure 4** designates the dose-volume limitations centered section, which encompasses all locations where no more than of 30% of the spinal cord volume may absorb dosages above 40 Gy. The analysis leads us to the conclusion that the dose-volume limitation is violated since 42.96% of the spinal cord area receives radiation dose over 40 Gy, as illustrated by the graph in **Figure 4**. However, after optimization, 22.98% of the spinal cord volume receives 40 Gy, so it fulfils the dose-volume bound.

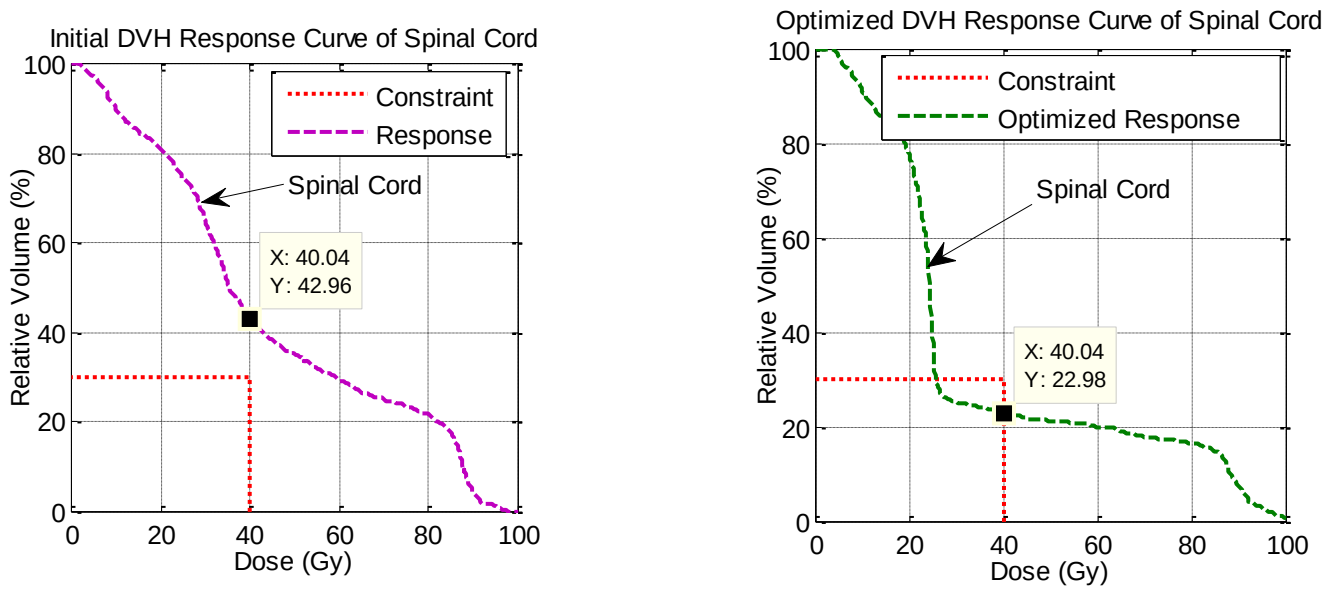

(a) **(b)**

Figure 4. DVH plot's upper and lower boundaries specify a 40 Gy overdose on 30% of the spinal cord volume. Left: Since 42.96% of the Spinal Cord, area received 40 Gy, so, the therapeutic strategy is unsuccessful. Right: As 22.98% of the Spinal Cord area received 40 Gy, so the therapeutic approach is successful.

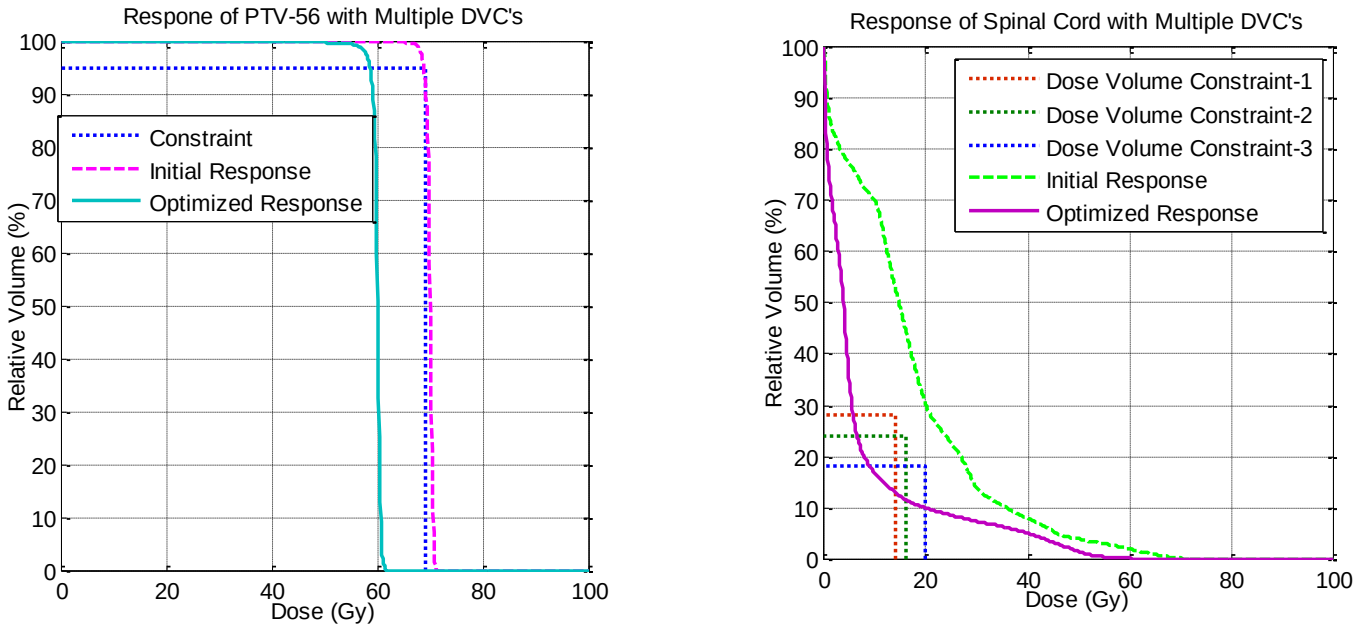

Figure 5. A comparison-based analysis for the multiple doses on OAR (Spinal Cord) where the dose-volume bounds approximately met, with 13.01% of the Spinal Cord volume received 14 Gy (52.61% initially), 11.57% of the Spinal Cord volume received 16 Gy (44.59% initially), and 9.94% of the Spinal Cord volume received 20 Gy (30.02% initially).

Single Target (PTV-56) and Critical Structure (Spinal Cord) with Multiple Dose-Volume Restrictions

We took into account our approach in this case for an individual target area (PTV-56) and an OAR (Spinal Cord) problem with multiple DVC's (**Figure 5**). Here we use internal ending deviation $\varepsilon^0 = 0.1$, weight adjustment factor $\tau = 2$, concluding deviation adjusting factor $\sigma = 0.95$, and external final deviation $\emptyset = 0.01$. A constant dose of 70 Gy is delivering to the target by considering that the surrounding healthy tissues mainly the liver should have the minimum effect for a multiple dose.

Table 1. Results of Multiple DVC's for the case of PTV-56 and Spinal Cord.

Parameter	PTV-56 D95 (Gy)	Spinal Cord %> 14 Gy	Spinal Cord %> 16 Gy	Spinal Cord %> 20 Gy	Time (Seconds)
Initialization	69.7	52.61	44.59	30.02	72.02
Optimized Response	61.24	13.01	11.57	9.94	178.61

In **Table 1**, we present the statistical findings of many dose-volume outcomes for PTV-56 and the spinal cord. An iterative solution-based optimization method formulated earlier is used for the generation of results. Since the standard D95 dosage for PTV-56 has been determined, the outcome is identical for every intended scenario. We have mathematically modeled the situation for three alternative dose-volume limitations (14 Gy, 16 Gy, and 20 Gy) in the context of the organ (spinal cord). There are specific variations in the magnitude of the response produced for every combination of the dose-volume restrictions. The initial response was converged in 72.02 seconds, whereas the optimized response was converged by utilizing the time of 178.61 seconds, as depicted in **Figure 6**.

As it is clear from the result, our algorithm approximately satisfied all the constraints, but at the cost of the number of iterations and solution time.

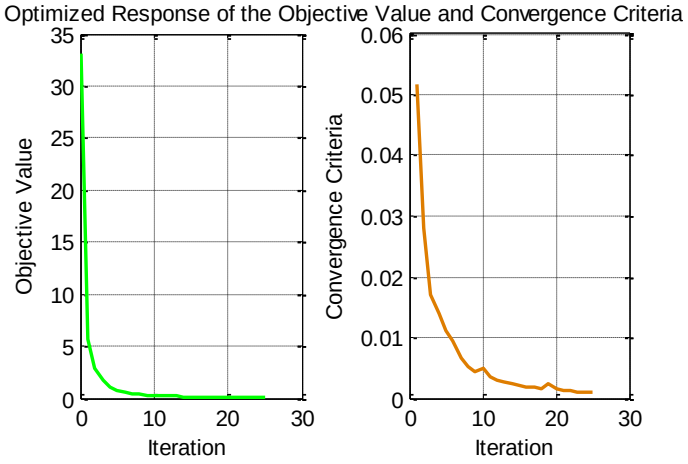

Figure 6. (a) Convergence curve for the values of objects. (b) The curve for the requirements of convergence

Test Results for Multiple Location Malignancy Cases

In each instance, we look into the situation by taking into consideration the substantial quantity of cancerous tissues (PTV) and normal tissues (OAR). Every time, we took into account the preliminary OAR weight $p_2^0 = 1$ and inner ending tolerance $\varepsilon^0 = 0.1$, together with the weight alter element of $\tau = 2$, the final threshold alter element of $\sigma = 0.95$, and the outside terminating tolerance of $\emptyset = 0.01$.

The most and least DVCs for each case must be listed on the PTV in order to administer the estimated dosages to the patients. **Table 2** displays the initial results of the analysis following a variety of baseline restrictions to PTVs and OARs. The overall response of the various target and critical organs is shown in **Figure 7**. We sought to achieve the best findings by applying the appropriate methods described before, and various dose-volume constraints were applied for the various OARs we analyzed here. Upon completion of the analysis, we observed that all of the OARs taken into consideration here roughly complied with the dose-volume constraints depicted in **Figure 7** and **Table 2**.

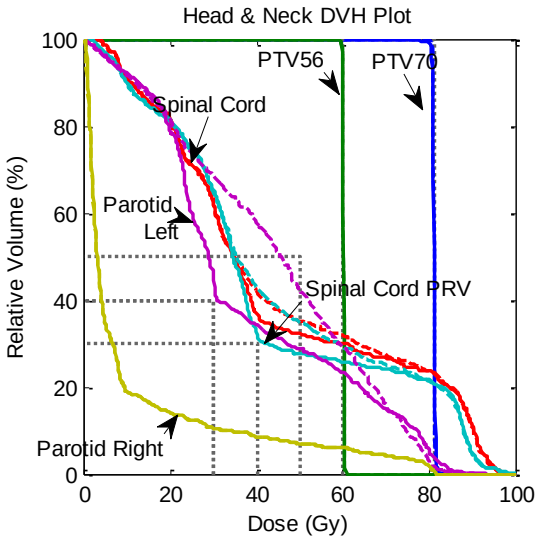

Figure 7. Target area and nearby vital organs' DVH responses, with the preliminary response shown as a dotted line and the optimized response as an intact line.

Table 2. DVH response for Head & Neck case for multiple location malignancy

Case	Target/ Critical Organs	Radiation beam delivered	Required % of delivery	Preliminary dose delivered	Optimized dose delivered	Period (Sec)
Head & Neck	PTV-70	82 Gy	100	81.58 (D95)	81.14 (D95)	254.28
	PTV-56	61 Gy	100	60.23 (D95)	60.12 (D95)	
	Spinal Cord	52 Gy	52	36.18	31.04	
	Spinal Cord PRV	40 Gy	32	41.82	30.11	
	Parotid Left	32 Gy	41	67.12	38.87	
	Parotid Right	32 Gy	41	61.32	11.42	

In **Figure 8**, the target value and requirements for convergence plots are displayed for each of the samples. The very first response for the Head & Neck met following 25 cycles with a target value of 8.3758 e-01 and a weight variance value of 9.8153 e-04, while the last response met following 24 cycles with a target value of 7.8362 e-01 and a weight variance value of 8.8295 e-04. The result is convergent for the remainder of the samples as well, meeting the condition. It should be mentioned that the L2 regularization factor is set at 1e-8 for the statistical analysis of each dataset.

It is quite challenging to meet all the required limitations adjacent to the target area and critical organs due to their close intimacy. It is desirable to use both the highest and lowest limits of the advised dosage due to the different structural difficulties and beam intensity patterns, that render it challenging to reach competitive targets as illustrated in **Figure 7**. Therefore, to ensure that all target and critical structures can receive the proper dose level. The majority of the OARs we have studied here fall under various dosing restrictions, and following the analysis, we determined that every critical structure we have taken into consideration is most likely to comply with dose volume restrictions.

Response by Varying the Value of Smoothness

From each smoothness stage to another, the optimization process keeps going unless it converges. We choose the value of the smoothness length m and the initialization for each subsequent stage as the key element for the subsequent optimization stages. The initialization process is dependent on the movement of the leaf combination, which moves with a constant speed while covering the entire area as the little leaves open. The prior result is used in the subsequent stages as the phase's starting value.

By definition, the quantity of objective-based solutions, assessed at the baseline operational level of smoothness (blue line), declines with CPU time for all algorithm phases. Beginning with the subsequent stage, the actual value of the aim is frequently developed together with the number of uniform goals. Furthermore, the corresponding effect on the immediate value may have an impact but is typically small whenever the enhancement in the smoothness value of the target is small. Although the value of the smooth object varies quickly when switching from one smooth stage to another, its exact value remains the same.

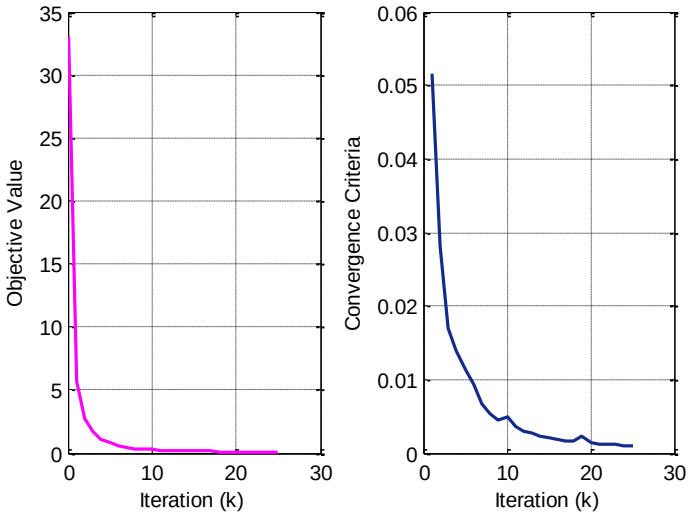

Figure 8. Convergence criteria plot and the objective value of the optimization procedure

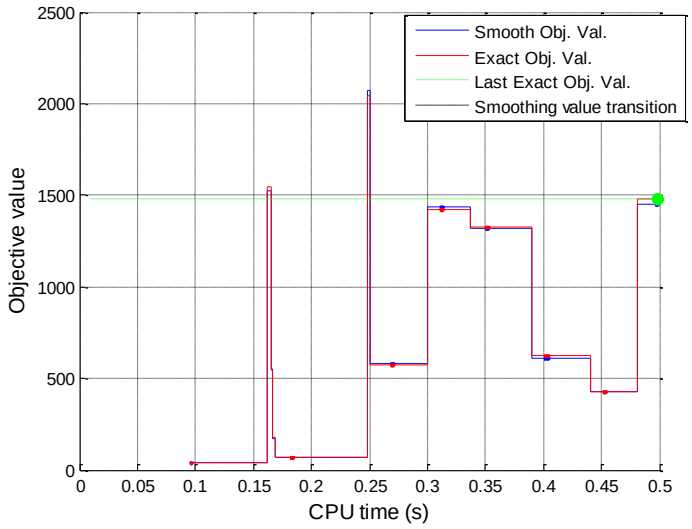

Figure 9. Comparative assessment of the performance of the objective value and processing time

Performance Assessment Parameters

The performance of the planned system is evaluated using different parameters. Points of interest for the parameters are clarified in **Table 3.**

The minimum dose (D_{min}), mean dose (D_{mean}), maximum dose (D_{max}), and estimated dosage to reach 95 percent of the target volume (D_{95}) were all evaluated for each target. To measure the design impacts on dosage delivery, the homogeneity index (HI), conformity index for the treatment area (CI), and S-index were computed.

Table 3. Performance evaluation parameter chart for proposed system

Parameter	Mathematical equation	Remarks
Homogeneity Index (H-Index)	$\frac{D_{\max}}{D_p}$	Conventionally used homogeneity index. D_{max} = Maximum Dose, D_p= Prescribed Dose
Homogeneity Index (HI-Index) [Formulae-1][41]	$\frac{D_5}{D_{95}}$	D_5 = Lowest dose in 5% of the treatment area D_{95} = Lowest dose in 95% of the treatment area
Homogeneity Index (HI-Index) [Formulae-2]	$\frac{D_{max}}{D_{min}}$	It represents the classical definition of HI. D_{max} = Maximum radiation in the treatment area D_{min} = Minimum radiation in the treatment area
Homogeneity Index (HI-Index) [Formulae-3][42]	$\frac{D_2 - D_{98}}{D_p}$	D_2 = Lowest dose in 2% of the treatment area D_{98} = Lowest dose in 98% of the treatment area D_p = Prescribed Dose
Homogeneity Index (HI-Index) [Formulae-4][43]	$\frac{D_5 - D_{95}}{D_p}$	D_5 = Lowest dose in 5% of the treatment area D_{95} = Lowest dose in 95% of the treatment area D_p = Prescribed Dose
Dose Homogeneity Index (DHI-Index)[44]	$\frac{D_{\geq 95\%(\text{within PTV})}}{D_{\geq 5\%(\text{within PTV})}}$	$D_{\geq 95\%}$ = Dose delivered in 95% of the treatment area. $D_{\geq 5\%}$ = Dose delivered in 5% of the treatment area.
S-Index[45]	$\sqrt{\frac{\sum[D_i - D_{mean}]^2 \times V_i}{V}}$	V_i= ith volume portion to receive a radiation of at least D_i. D_{mean}= mean dose V =Entire area

Table 4. Variation in the radiation dosage levels and the corresponding percentage accuracy

Cases	Formula	Lowest value	Highest value	Mean value	Median value	Mode	% Accuracy
Head & Neck	D_5/D_{95}	1.05	1.62	1.16	1.12	1.07	94.12%
	D_{max}/D_{min}	1.09	9.52	2.14	1.82	1.72	92.88%
	$\frac{D_2 - D_{98}}{D_p}$	0.07	0.75	0.25	0.17	0.11	93.12%
	$\frac{D_5 - D_{95}}{D_p}$	0.08	0.85	0.21	0.15	0.08	93.95%
	D_{max}/D_p	1.08	2.02	1.22	1.27	1.20	88.57%
	S-index	0.67	20.32	4.52	3.82	1.53	97.62%

Computation of performance parameters

When it comes to measuring the performance or accuracy of a certain model or prediction, various computations are often used. One essential aspect of this is considering the target volume, which refers to the actual value or outcome being predicted. Several measures can be utilized to assess the accuracy of predictions with respect to the target volume. The minimum represents the lowest predicted value, while the maximum indicates the highest predicted value. The mean gives the average value of all predictions, providing an overall estimate of the target volume. The median, on the other hand, identifies the middle value of the predictions, which is particularly useful when outliers are present. Additionally, the mode denotes the most frequently occurring predicted value. Lastly, the percentage accuracy is computed by comparing the predicted values to the actual target volume, thereby quantifying the level of correctness of the predictions. By considering these different computations, one can gain a comprehensive understanding of how well a model performs in predicting the target volume.

We are showing the variation in the radiation dosage levels using different formulations and the corresponding percentage accuracy in case of head & neck malignancy in **Table 4**.

Conclusion

There are numerous objectives and limits on the PTVs and OARs that must be satisfied when solving the fluence-mapping problem. The clinically pertinent DVH for the fluence map problem is NP-hard since the majority of the problem is non-convex. The fundamental objective of radiotherapy and other radiation-based therapy plans is to give the malignant cells the appropriate dosage while sparing the surrounding tissues from damage. The stated problem was solved using iteration-based approaches. There are several subsections in the problem analysis. In order to begin analysing the issue, only one PTV and one OAR were taken into account. As the problem's complexity grew, more PTV and OAR were added, and additional DVCs were also applied to them. Here, we present a model-based approach that may generate plans for treatment that fully satisfy the constraints on dose volume for OARs without relying on any unproven methods. With similar plan features across several treatment planners, this recommended method can produce global minima for IMRT plans and effectively improve safety for substantial dual OARs. As demonstrated by examples using the CORT dataset, the entire technique has the capacity to address varied objectives and produce efficient treatment procedures.

Conflict of interest

There is no conflict of interest. This research did not receive any specific grant from funding agencies in the public, commercial, or not-for-profit sectors.

References

1. Bray F, Ferlay J, Soerjomataram I, Siegel RL, Torre LA, Jemal A. Global cancer statistics 2018: GLOBOCAN estimates of incidence and mortality worldwide for 36 cancers in 185 countries. CA A Cancer J Clinicians. 2018;68(6):394-424. https://doi.org/10.3322/caac.21492
2. Ferlay J, Soerjomataram I, Dikshit R, et al. Cancer incidence and mortality worldwide: Sources, methods and major patterns in GLOBOCAN 2012. Intl Journal of Cancer. 2014;136(5). https://doi.org/10.1002/ijc.29210
3. Kufta K, Forman M, Swisher-McClure S, Sollecito TP, Panchal N. Pre-Radiation dental considerations and management for head and neck cancer patients. Oral Oncology. 2018;76:42-51. https://doi.org/10.1016/j.oraloncology.2017.11.023
4. Duarte VM, Liu YF, Rafizadeh S, Tajima T, Nabili V, Wang MB. Comparison of Dental Health of Patients with Head and Neck Cancer Receiving IMRT vs Conventional Radiation. Otolaryngol--head neck surg. 2013;150(1):81-86. https://doi.org/10.1177/0194599813509586
5. Singh P, Tripathi S, Gupta S. A unified approach for optimal dose delivery and trajectory optimization for the treatment of prostate cancer. Biomedical Signal Processing and Control. 2021;69:102884. https://doi.org/10.1016/j.bspc.2021.102884
6. Singh P, Tripathi S, Tamrakar RK. Fluence map optimisation for prostate cancer intensity modulated radiotherapy planning using iterative solution method. Polish Journal of Medical Physics and Engineering. 2020;26(4):201-209. https://doi.org/10.2478/pjmpe-2020-0024
7. Lim GJ, Choi J, Mohan R. Iterative solution methods for beam angle and fluence map optimization in intensity modulated radiation therapy planning. OR Spectrum. 2007;30(2):289-309. https://doi.org/10.1007/s00291-007-0096-1
8. Paradis E, Cao Y, Lawrence TS, et al. Assessing the Dosimetric Accuracy of Magnetic Resonance-Generated Synthetic CT Images for Focal Brain VMAT Radiation Therapy. International Journal of Radiation Oncology*Biology*Physics. 2015;93(5):1154-1161. https://doi.org/10.1016/j.ijrobp.2015.08.049
9. Breedveld S, Storchi PRM, Keijzer M, Heijmen BJM. Fast, multiple optimizations of quadratic dose objective functions in IMRT. Phys Med Biol. 2006;51(14):3569-3579. https://doi.org/10.1088/0031-9155/51/14/019
10. Censor Y, Ben-Israel A, Xiao Y, Galvin JM. On linear infeasibility arising in intensity-modulated radiation therapy inverse planning. Linear Algebra and its Applications. 2008;428(5-6):1406-1420. https://doi.org/10.1016/j.laa.2007.11.001
11. Singh P, Tripathi S, Tamrakar RK. Dose-Volume Constraints Based Inverse Treatment Planning For Optimizing the Delivery of Radiation Therapy. GOR. 2020;33(03). https://doi.org/10.37896/gor33.03/489
12. Cotrutz C, Xing L. Using voxel-dependent importance factors for interactive DVH-based dose optimization. Phys Med Biol. 2002;47(10):1659-1669. https://doi.org/10.1088/0031-9155/47/10/304
13. Gutiontov SI, Shin EJ, Lok B, Lee NY, Cabanillas R. Intensity-modulated radiotherapy for head and neck surgeons. Head & Neck. 2015;38(S1). https://doi.org/10.1002/hed.24338
14. Zaghian M, Lim G, Liu W, Mohan R. An Automatic Approach for Satisfying Dose-Volume Constraints in Linear Fluence Map Optimization for IMPT. JCT. 2014;05(02):198-207. https://doi.org/10.4236/jct.2014.52025
15. Jin R, Min Z, Song E, Liu H, Ye Y. A novel fluence map optimization model incorporating leaf sequencing constraints. Phys Med Biol. 2010;55(4):1243-1264. https://doi.org/10.1088/0031-9155/55/4/023
16. Rocha H, Dias JM, Ferreira BC, Lopes MC. Combinatorial optimization for an improved transition from fluence optimization to fluence delivery in IMRT treatment planning. Optimization. 2012;61(8):969-987. https://doi.org/10.1080/02331934.2011.607498
17. Jin R, Min Z, Song E, Liu H, Ye Y. A novel fluence map optimization model incorporating leaf sequencing constraints. Phys Med Biol. 2010;55(4):1243-1264. https://doi.org/10.1088/0031-9155/55/4/023
18. Wu X, Hou Y, Zhang K. Switched system optimal control approach for drug administration in cancer chemotherapy. Biomedical Signal Processing and Control. 2022;75:103575. https://doi.org/10.1016/j.bspc.2022.103575
19. Schmidt M, Berg E, Friedlander M, Murphy K. Optimizing costly functions with simple constraints: A limited-memory projected quasi-newton algorithm. In: Proceedings of the Twelfth International Conference on Artificial Intelligence and Statistics, PMLR 5:456-463, 2009.
20. Singh P, Mishra A, Mishra SK. A comprehensive analysis of the challenges and potential side effects of radiation therapy for palliative cancer treatment. Médecine Palliative. 2024;23(2):75-91. https://doi.org/10.1016/j.medpal.2023.12.002

21. Rosen II, Lane RG, Morrill SM, Belli JA. Treatment plan optimization using linear programming. Medical Physics. 1991;18(2):141-152. https://doi.org/10.1118/1.596700
22. Fu A, Ungun B, Xing L, Boyd S. A convex optimization approach to radiation treatment planning with dose constraints. Optim Eng. 2018;20(1):277-300. https://doi.org/10.1007/s11081-018-9409-2
23. Mukherjee S, Hong L, Deasy JO, Zarepisheh M. Integrating soft and hard dose-volume constraints into hierarchical constrained IMRT optimization. Medical Physics. 2019;47(2):414-421. https://doi.org/10.1002/mp.13908
24. Schlegel W. New Technologies in 3D Conformal Radiation Therapy: Introduction and Overview. Medical Radiology.:1-6. https://doi.org/10.1007/3-540-29999-8_1
25. Xu Y, Diwanji T, Brovold N, et al. Assessment of daily dose accumulation for robustly optimized intensity modulated proton therapy treatment of prostate cancer. Physica Medica. 2021;81:77-85. https://doi.org/10.1016/j.ejmp.2020.11.035
26. Shepard DM, Ferris MC, Olivera GH, Mackie TR. Optimizing the Delivery of Radiation Therapy to Cancer Patients. SIAM Rev. 1999;41(4):721-744. https://doi.org/10.1137/s0036144598342032
27. Cotrutz C, Lahanas M, Kappas C, Baltas D. A multiobjective gradient-based dose optimization algorithm for external beam conformal radiotherapy. Phys Med Biol. 2001;46(8):2161-2175. https://doi.org/10.1088/0031-9155/46/8/309
28. Aubry J, Beaulieu F, Sévigny C, Beaulieu L, Tremblay D. Multiobjective optimization with a modified simulated annealing algorithm for external beam radiotherapy treatment planning. Medical Physics. 2006;33(12):4718-4729. https://doi.org/10.1118/1.2390550
29. Shou Z, Yang Y, Cotrutz C, Levy D, Xing L. Quantitation of thea prioridosimetric capabilities of spatial points in inverse planning and its significant implication in defining IMRT solution space. Phys Med Biol. 2005;50(7):1469-1482. https://doi.org/10.1088/0031-9155/50/7/010
30. Spirou SV, Chui C. A gradient inverse planning algorithm with dose-volume constraints. Medical Physics. 1998;25(3):321-333. https://doi.org/10.1118/1.598202
31. Taylor A. Intensity-modulated radiotherapy - what is it? Cancer Imaging. 2004;4(2):68-73. https://doi.org/10.1102/1470-7330.2004.0003
32. He H, Wu D. Transfer Learning for Brain–Computer Interfaces: A Euclidean Space Data Alignment Approach. IEEE Trans Biomed Eng. 2020;67(2):399-410. https://doi.org/10.1109/tbme.2019.2913914
33. Sorea MŞ. Measuring the local non-convexity of real algebraic curves. Journal of Symbolic Computation. 2022;109:482-509. https://doi.org/10.1016/j.jsc.2020.07.017
34. Kim J, Shin J, Yang I. Hamilton-Jacobi deep Q-Learning for deterministic continuous-time systems with lipschitz continuous control., The Journal of Machine Learning Research. 2021:22(1):9363-9396.
35. Gebrie AG. Distributed accelerated proximal conjugate gradient methods for multi-agent constrained optimization problems. Published online 2023. https://doi.org/10.48550/ARXIV.2306.04230
36. Cobos-Carbó A. Ensayos clínicos aleatorizados (CONSORT). Medicina Clínica. 2005;125:21-27. https://doi.org/10.1016/s0025-7753(05)72205-3
37. Craft D, Bangert M, Long T, Papp D, Unkelbach J. Shared data for intensity modulated radiation therapy (IMRT) optimization research: the CORT dataset. GigaSci. 2014;3(1). https://doi.org/10.1186/2047-217x-3-37
38. Grant M, Boyd S. CVX: Matlab software for disciplined convex programming, version 2.1. 2014. Available at: https://cvxr.com/cvx2
39. Jiaolong Xu, Ramos S, Vazquez D, Lopez AM. Domain Adaptation of Deformable Part-Based Models. IEEE Trans Pattern Anal Mach Intell. 2014;36(12):2367-2380. https://doi.org/10.1109/tpami.2014.2327973
40. Singh P, Singh S, Mishra A, Mishra SK. Multimodality treatment planning using the Markov decision process: a comprehensive study of applications and challenges. Res Biomed Eng. 2024;40(2):435-450. https://doi.org/10.1007/s42600-024-00349-4
41. Semenenko VA, Reitz B, Day E, Qi XS, Miften M, Li XA. Evaluation of a commercial biologically based IMRT treatment planning system. Medical Physics. 2008;35(12):5851-5860. https://doi.org/10.1118/1.3013556
42. Wu Q, Mohan R, Morris M, Lauve A, Schmidt-Ullrich R. Simultaneous integrated boost intensity-modulated radiotherapy for locally advanced head-and-neck squamous cell carcinomas. I: dosimetric results. International Journal of Radiation Oncology*Biology*Physics. 2003;56(2):573-585. https://doi.org/10.1016/s0360-3016(02)04617-5
43. Spiotto MT, Weichselbaum RR. Comparison of 3D Confromal Radiotherapy and Intensity Modulated Radiotherapy with or without Simultaneous Integrated Boost during Concurrent Chemoradiation for Locally Advanced Head and Neck Cancers. Camphausen K, ed. PLoS ONE. 2014;9(4):e94456. https://doi.org/10.1371/journal.pone.0094456
44. Petrova D, Smickovska S, Lazarevska E. Conformity Index and Homogeneity Index of the Postoperative Whole Breast Radiotherapy. Open Access Maced J Med Sci. 2017;5(6):736-739. https://doi.org/10.3889/oamjms.2017.161
45. Yoon M, Park SY, Shin D, et al. A new homogeneity index based on statistical analysis of the dose–volume histogram. J Applied Clin Med Phys. 2007;8(2):9-17. https://doi.org/10.1120/jacmp.v8i2.2390

46. Lim GJ, Choi J, Mohan R. Iterative solution methods for beam angle and fluence map optimization in intensity modulated radiation therapy planning. OR Spectrum. 2007;30(2):289-309. https://doi.org/10.1007/s00291-007-0096-1

47. Vandenbroucke JP, von Elm E, Altman DG, et al. Strengthening the Reporting of Observational Studies in Epidemiology (STROBE): Explanation and Elaboration. PLoS Med. 2007;4(10):e297. https://doi.org/10.1371/journal.pmed.0040297

48. Page MJ, McKenzie JE, Bossuyt PM, et al. The PRISMA 2020 statement: an updated guideline for reporting systematic reviews. BMJ. Published online March 29, 2021:n71. https://doi.org/10.1136/bmj.n71

49. Riley DS, Barber MS, Kienle GS, et al. CARE guidelines for case reports: explanation and elaboration document. Journal of Clinical Epidemiology. 2017;89:218-235. https://doi.org/10.1016/j.jclinepi.2017.04.026